Journal of Power Sources 450 (2020) 227661

Contents lists available at ScienceDirect

Journal of Power Sources

journal homepage: www.elsevier.com/locate/jpowsour

Pyrite-type cobalt phosphosulphide bifunctional catalyst for aqueous and gel-based rechargeable zinc-air batteries

Bratati Roy [1], K.J. Shebin [1], S. Sampath [*]

Department of Inorganic and Physical Chemistry, Indian Institute of Science, Bangalore, 560012, India

HIGHLIGHTS

- Large, high-quality CoPS crystals have been synthesized by solid-state synthesis.
- Synergism between P and S makes it an excellent bifunctional electrocatalyst.
- Primary and rechargeable zinc-air batteries in aqueous and gel electrolytes demonstrated.
- Power density, efficiency and stability of CoPS outperforms noble metal catalysts.

GRAPHICAL ABSTRACT

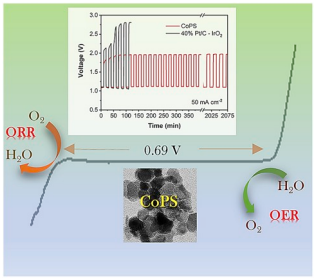

ARTICLE INFO

Keywords:
Pyrite-type cobalt phosphosulphide
Oxygen reduction reaction
Oxygen evolution reaction
Liquid and gel electrolytes
Rechargeable zinc-air batteries

ABSTRACT

Bifunctional electrocatalysts with favorable electrode kinetics towards oxygen reduction and oxygen evolution reactions are the main pre-requisites to achieve practical utility of metal-air systems. Herein, ternary pyrite type nanosized cobalt phosphosulphide is reported as an excellent oxygen reduction/oxygen evolution catalyst in alkaline medium with a favorable reversible oxygen electrode index (difference between E_{10mA} for oxygen evolution and E_{3mA} for oxygen reduction) of 0.69 V. Four-electron reduction with low overpotential of ~240 mV to observe a current density of 10 mA cm^{-2} is reported. The assembled zinc-air batteries with both aqueous liquid- and gel-based electrolytes display stable low charge-discharge voltage polarization over a long duration. Aqueous primary zinc-air battery exhibits an impressive peak power density of 385 mW cm^{-2} at 560 mA cm^{-2} and a current density of 220 mA cm^{-2} at 1.0 V. The zinc-air battery in the air-breathing, rechargeable mode operates for over 100 h at 10 mA cm^{-2} and over a few hundred cycles under a drain current of 50 mAcm^{-2}. The rechargeable battery has been investigated for both long term (4 h) and short term (10 min) cycles under different drain currents (10, 20 and 50 mA cm^{-2}). Round trip efficiencies of ~64% have been achieved. Use of CoPS electrodes with gel-based electrolytes has also been demonstrated. The primary gel battery displays a specific capacity of 803 mA cm^{-2} corresponding to an energy density of 891 Wh kg^{-1}. The high efficiency and durability of the catalyst establish its feasibility as a cost-effective alternative to precious metal catalysts.

* Corresponding author.
E-mail address: sampath@iisc.ac.in (S. Sampath).
[1] BR and SKJ contributed equally to the work.

https://doi.org/10.1016/j.jpowsour.2019.227661
Received 16 August 2019; Received in revised form 12 December 2019; Accepted 23 December 2019
Available online 1 January 2020

1. Introduction

With the advent of new generation electronic devices along with large energy demands of the grid storage, there is a need for high-density energy storage and conversion systems [1–3]. These devices need rechargeable batteries with energy densities higher than the commercial lithium ion batteries that yield specific energies of 265 Wh kg^{-1} [4,5]. This has led to immense growth in the research of secondary metal-air batteries (Zn, Li, Mg, Al, Fe, Na, K - based), which have been found to possess higher energy densities than several known metal-ion batteries [6–10]. High energy density zinc-air batteries have been found to be promising due to safety, easy processability and abundance of zinc metal. Primary zinc-air battery technology is quite well established, but the development of high-performance rechargeable zinc-air batteries has been restricted by sluggish kinetics and high overpotential of oxygen reduction reaction (ORR) and the oxygen evolution reactions (OER) [11]. Currently, the best known catalysts for the oxygen electrode reactions are Pt, its alloys and its variants for ORR and Ir/Ru oxides for OER in alkaline medium [12–15]. There is a need to develop inexpensive and abundant bifunctional electrocatalysts with low overpotential for both ORR and OER.

In this direction, several transition metal oxides have been reported as bifunctional electrocatalysts [16–20]. Attention has recently shifted to transition metal chalcogenides (TMCs) [21–23] and transition metal phosphides (TMPs) [24–27], due to their favorable electronic structure and multifunctional electrocatalytic activities. The TMCs, despite their high electrochemical stability, suffer from relatively poor electrocatalytic activity, especially in alkaline medium [28,29] while TMPs, which are being investigated as alternative non-precious catalysts, show high catalytic activity but inferior stability [30,31]. Effective strategy to improve their electrochemical performance is to use either bimetallic TMCs/TMPs [32–35] or to dope phosphorus (P)/sulphur (S) [36–38] along with different carbon supports [39–41]. Substitution of P/S leads to a synergistic effect between sulphur and phosphorus and has been shown to improve both electrochemical activity and stability in various matrices. This argument is substantiated by the fact that MoP|S [42], MoS_2–MoP core-shell structures [43], and $MoS_{2(1-x)}P_x$ solid solutions [44] exhibit better hydrogen evolution reaction (HER) activity than that of pure sulphide or the phosphide. Furthermore, P doped MoS_2 nanosheets have been found to show higher ORR activity than that of pristine MoS_2 [45].

In the search for feasible alternatives to precious metal catalysts (Pt, Ir, and Ru based compounds), Co-based catalysts have emerged as a class of promising electrocatalysts due to their abundance, relatively low cost, effectiveness and robustness of the electrodes [22,26,33,34,39,40,46]. These catalysts including sulphides (e.g. Co_9S_8) and phosphate-based systems (e.g. Co-Pi catalysts) [47–49], exhibit good bifunctional activity towards ORR/OER. Recently, ternary pyrite type CoPS has been introduced as a catalyst that exhibits exceptional HER activity with a very low overpotential of 48 mV @ 10 $mAcm^{-2}$ [50]. Liu and co-workers have reported very good OER activities based on $Co_{2-x}SP$/CFP electrocatalyst [51]. Quaternary pyrite type $Ni_{1.0}Co_{2.05}P_{5.26}S_{0.65}$ [52] and hexagonal phase pyrrhotite-type $Co_{0.9}S_{0.58}P_{0.42}$ [53] have been found to catalyze water splitting reaction showing remarkable bifunctionality towards HER/OER. Incorporation of a less electronegative element, P by substituting S in the pyrite type lattice leads to enhanced covalency in metal-ligand bonds [43]. This helps in preventing sulphide oxidation and metal dissolution leading to increased stability and durability of the catalyst. The OER activity of the phosphosulphides in alkaline electrolytes is attributed to the in-situ generation of cobalt oxy/hydroxy species and favorable P/S ratio to maximize the Co^{3+}/Co^{2+} fraction [53]. Presence of metal in +3 state increases the electron accepting tendency of the metal ion for OER in alkaline medium enabling superior electrocatalysis.

As given above, phosphosulphides particularly cobalt-based ones, have gained attention as excellent water-splitting catalysts and are expected to have multifunctional behavior. The ORR activity of these materials is yet to be explored. In the present studies, CoPS is investigated for its oxygen reduction ability and indeed, it is found to be highly active with favorable four electron process. Combined with the exceptional oxygen evolution activity, it is used as a bifunctional air-cathode catalyst for both primary and rechargeable zinc-air batteries in aqueous alkaline electrolytes. Both liquid- and gel-based electrolytes in combination with CoPS are observed to exhibit excellent and very stable performance.

2. Experimental section

2.1. Synthesis and characterization

CoPS was synthesized by a solid-state reaction procedure using stoichiometric amounts of cobalt (Sigma-Aldrich, 99.9%), phosphorous (Alfa Aesar, 99.9%) and sulphur (Aldrich, 99.98%). Briefly, the as-obtained cobalt powder was pre-treated at 300 °C under hydrogen atmosphere for 5 h to remove any remnant oxide. The elements were then ground using mortar and pestle and pressed into a pellet. The temperature program used for the synthesis of CoPS crystals is given in the supporting information. The as-synthesized material was characterized using X-ray diffraction and electron microscopy (Bruker D8 ADVANCE diffractometer, Carl Zeiss Ultra 55 scanning electron microscope and JEOL JEM 2100F transmission electron microscope). High-resolution XPS measurements were carried (Kratos Axis Ultra DLD X-ray photoelectron spectrometer) with monochromatic Al kα radiation. Raman spectroscopy was carried out at an excitation wavelength of 514.5 nm (LabRAM HR (UV) instrument).

2.2. Electrode preparation and electrochemical measurements

A conventional three-electrode cell was used in conjunction with a potentiostat/galvanostat (CH660C, CH Instruments, USA). The catalyst ink was prepared by dispersing 4 mg of the catalyst in 1 mL of isopropanol-water mixture (1:1) along with 5 μL of 5 wt % Nafion. 5 μL of the ink was drop cast onto a glassy carbon electrode of 3 mm diameter to obtain a catalyst loading of 0.28 mg cm^{-2}. Pt foil and Hg/HgO (MMO) electrodes were used as counter and reference electrodes respectively. The reference electrode was calibrated, and all the potentials are reported with respect to the reversible hydrogen electrode (RHE). Before each experiment, the electrolyte, 0.5 M KOH was purged with high purity N_2 for 30 min and further with high purity O_2 for 30 min in the case of ORR experiments. A steady blanket of O_2 above the liquid electrolyte was maintained during the experiment. Linear sweep voltammograms were recorded (with iR compensation) at 1 mV s^{-1} for OER and at 5 mV s^{-1} for ORR.

2.3. Zinc-air battery fabrication

A catalyst ink was prepared by grinding CoPS (65 wt%) with acetylene black (25 wt%) as the carbon support and 5 wt % Nafion (10 wt %) as a binder in N-methyl-2-pyrrolidone (NMP). The ink was loaded onto a gas diffusion layer (GDL) and used as air-cathode. A two-electrode configuration was used for primary cells, where a polished zinc foil (Alfa Aesar) was used as the anode and catalyst loaded on GDL (1 mg cm^{-2} CoPS) was used as the cathode. For rechargeable cells, a parallel tri-electrode configuration was used with zinc as the anode and the same catalyst, CoPS on GDL as both air cathodes kept on either side of the zinc plate. Mass loadings of 1 mg cm^2 for ORR and 2 mg cm^2 for OER were used. In liquid-based batteries, the electrolyte used was 6 M KOH in primary cell configuration and the alkali along with 0.2 M zinc acetate in the rechargeable mode. A continuous supply of moist O_2 was maintained during the operation of the batteries unless mentioned otherwise. The gel-based battery was assembled using a gel electrolyte based on potassium salt based poly(acrylic acid) (PAAK). It was prepared by the

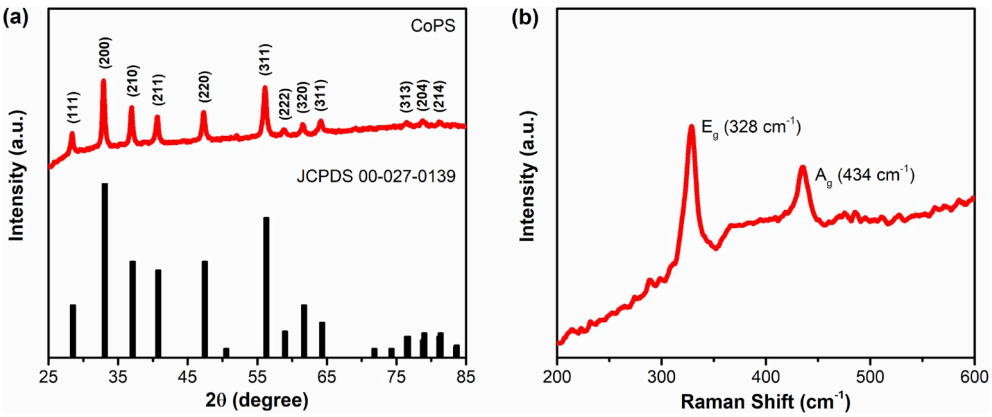

Fig. 1. (a). X-ray diffraction pattern of CoPS. The standard pattern is also shown (JCPDS 00-027-0139). (b) Raman spectrum showing the E_g and A_g bands of the chalcogenide dumbbell in the pyrite lattice of CoPS. Wavelength of the laser used is 514 nm.

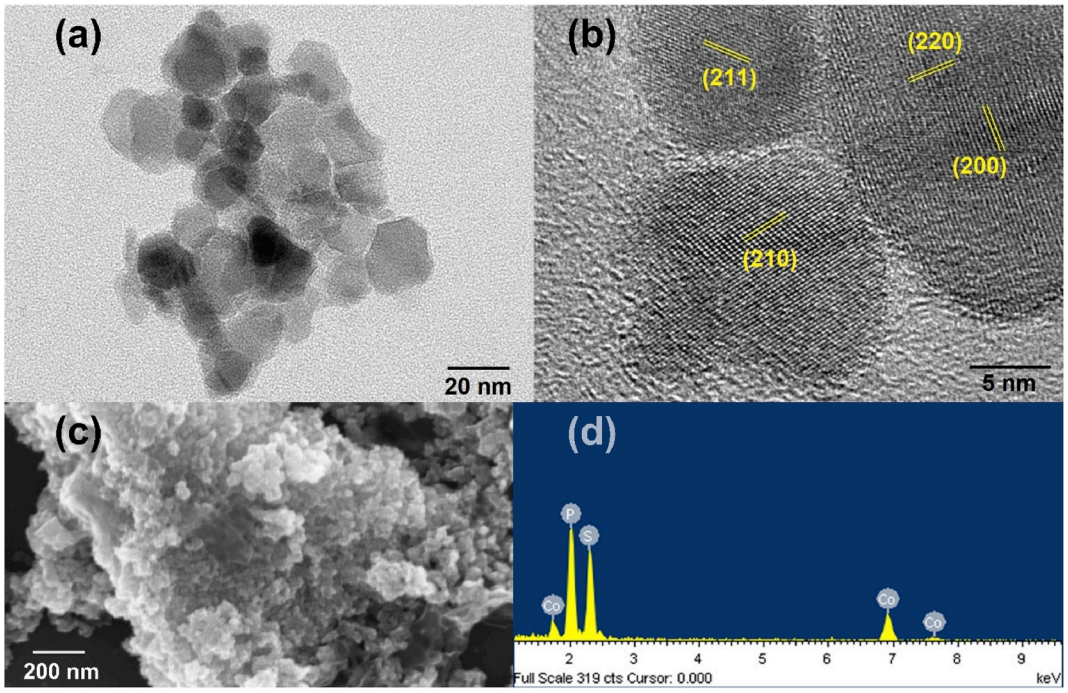

Fig. 2. (a). Transmission electron microscopic image of CoPS nanoparticles. (b) High resolution picture showing different exposed (hkl) planes. (c). Scanning electron microscopic image of bulk CoPS showing agglomeration. (d) EDS spectrum of individual elements (1:1:1 of Co:P:S).

addition of 7 wt % of PAAK to 6 M KOH with stirring [54]. The gel was allowed to settle overnight and subsequently transferred to a closed plastic container with inlets for the electrodes. The electrodes were inserted into the gel and one side of the container was pierced with holes for air flow in the ORR side. All the experiments were performed in air breathing mode.

3. Results and discussion

The catalyst, CoPS is synthesized using solid state preparation techniques and characterized using spectroscopic and microscopic techniques. This is followed by the static and hydrodynamic voltammetry to understand the kinetics of ORR and OER. Subsequently, the catalyst is used for rechargeable zinc-air batteries in alkaline liquid and gel electrolytes.

3.1. Physicochemical characterization

The as-synthesized pyrite-type CoPS is dark grey in color. The material is highly crystalline and the observed diffraction peaks (Fig. 1a) are assigned to CoPS (JCPDS file number 00-027-0139) corresponding to the cubic system (a = 5.422 Å). In the confocal Raman spectrum (Fig. 1b), two peaks are observed at 328 cm^{-1} and 434 cm^{-1} which are due to the characteristic vibrational modes of libration and in-phase stretching of S–S dumbbells in a pyrite lattice [50].

Bright-field transmission electron microscopy (TEM) images (Fig. 2a and b) show the morphology of CoPS nanoparticles to be a cubic with an approximate size of 20 nm. In the high-resolution TEM (HRTEM) images, lattice spacings of 2.71, 2.44, 2.41 and 1.90 nm are measured and are indexed to (200), (210), (211) and (220) planes of CoPS. The morphology as observed in the SEM image (Fig. 2c), shows agglomeration of porous CoPS nanoparticles in bulk state. The EDS data indicates the presence of Co, P, and S in the ratio 1:1:1 as given in Fig. 2d.

X-ray photoelectron spectroscopy measurements have been

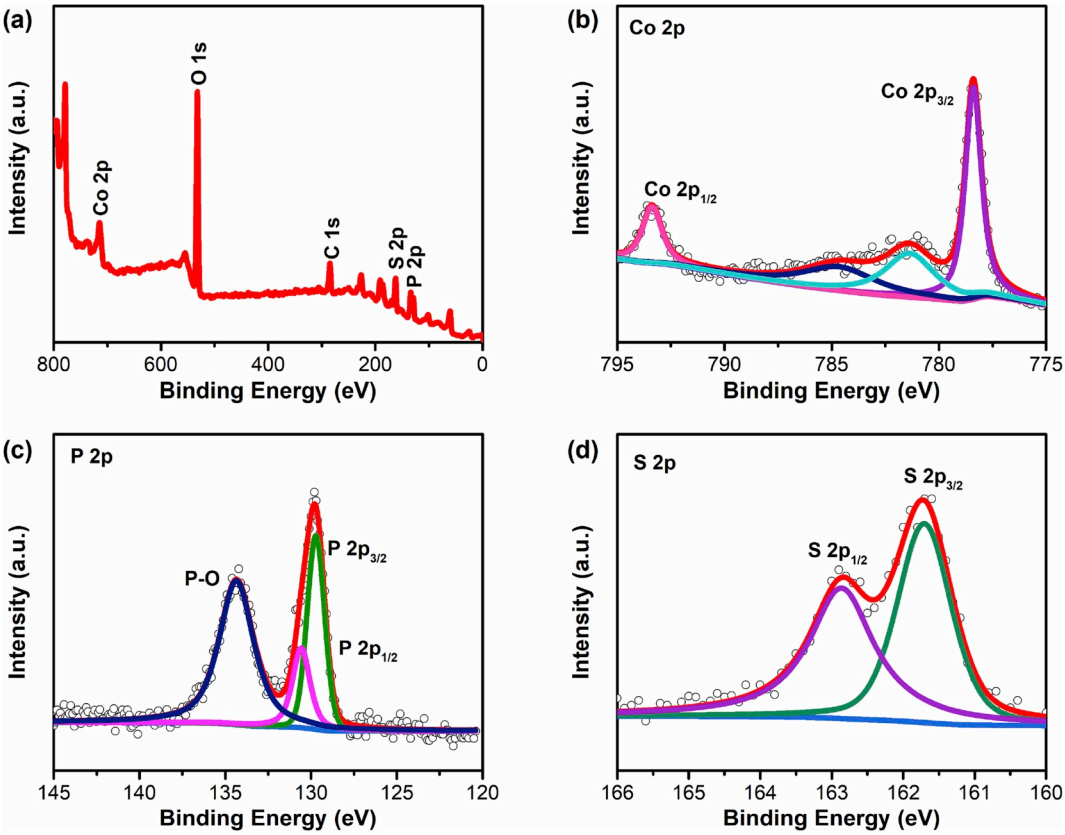

Fig. 3. X-ray photoelectron spectra of CoPS. (a) Survey spectrum for CoPS. High resolution XPS peaks for 2p core levels of Co (b), P (c) and S (d) are shown. The deconvolution is also shown.

performed to investigate the surface chemical state and composition of the electrocatalyst. The survey spectrum (Fig. 3a) demonstrates the presence Co, P, S, C and O. It is known that the oxidation state of Co is 3 + and S and P are notionally in −1 and −2 states respectively [50]. CoPS contains Co3+ octahedra and dumbbells of S/P homogeneously distributed in the lattice (Fig. 1 in reference 50). In the present studies, the high-resolution XPS spectral region of Co (Fig. 3b) shows Co 2p core level peaks with binding energies of Co $2p_{3/2}$ and Co $2p_{1/2}$ at 778.8 eV and 793.8 eV respectively. A single doublet without any further splitting is indicative of spin paired electronic configuration confirming the presence of cobalt in +3 oxidation state [50,55,56]. Two regions (Fig. 3c) are observed for phosphorous. The region centered at 129.8 eV could be deconvoluted into two peaks with binding energies of 129.7 eV and 130.6 eV corresponding to P $2p_{3/2}$ and P $2p_{1/2}$ levels of phosphide species. Additionally, a peak corresponding to P–O bond of surface oxidized phosphate species is observed at 133.4 eV. This is commonly noticed in metal phosphides and phosphosulphides under ambient atmosphere [52,57]. A doublet is observed in the S 2p region (Fig. 3d) at 162.1 eV and 163.3 eV corresponding to S $2p_{3/2}$ and S $2p_{1/2}$ levels respectively. The elemental composition of the catalyst is found to be consistent with the CoPS composition.

3.2. Electrochemical characterization

3.2.1. Oxygen reduction reaction

Initial studies to establish the ability of CoPS to reduce O_2 in alkaline medium is carried using cyclic voltammetry of CoPS coated GCE in 0.5 M KOH at a scan rate of 10 mV s^{-1}. The onset of a peak at 0.80 V vs RHE (Fig. 4a) in the presence of O_2 indicates the activity of CoPS towards ORR. ORR can occur via either a single step 4 electron pathway or a two-step 2 electron pathway (SI) [58–60]. The second pathway involves the generation of H_2O_2 reducing the efficiency and hence is less preferred. The Tafel slopes obtained from mass transport corrected polarization plots (Fig. 4b) at 1600 rpm are 60 mV dec^{-1} at low current density (Temkin adsorption) and 127 mV dec^{-1} at high current density (Langmuir adsorption) regions. The values are comparable to that observed on Pt/C (~60 mV dec^{-1} and 120 mV dec^{-1} at low and high current densities respectively) [37,58,61]. Parallel K-L plots (Fig. 4d) with linear characteristics at different potentials are indicative of first-order reaction kinetics. The number of electrons involved in the reduction reaction is calculated to be ~3.6 in the potential range 0.65 to 0.35 V vs RHE (Figs. S3a and SI). The kinetic parameters of current density and the rate constant values (Figs. S3b and SI) are similar to those reported for transition metal oxides, hydroxides and chalcogenides [62–65].

RRDE studies have been performed using an Au–Pt electrode in which CoPS is drop casted on the Au disk. The Pt ring electrode used to oxidize the ORR generated peroxide species is set at - 0.6 V vs MMO. The ring collection efficiency is determined to be 0.238 using reversible ferricyanide/ferrocyanide redox couple. From the ratio of disc current (I_d) to ring current (I_R) (Fig. 5a), the number of electrons involved in the reduction of O_2 is determined to be 3.8 at a potential of - 0.8 V vs MMO (Fig. 5b). The H_2O_2 percentage is found to be 8.4%. The small quantity of peroxide generated confirms the reduction of O_2 to H_2O through the preferred one step, four-electron pathway. The stability of the catalyst is assessed by chronoamperometry where the potential is held at 0.69 V vs RHE for a duration of 10 h (Figs. S8b and SI). Apart from the initial change in current due to equilibration, no appreciable change is observed for several hours, indicating very good durability of the catalyst.

3.2.2. Oxygen evolution reaction

The oxygen evolution activity of the electrocatalyst is analyzed in 0.5 M KOH using a three-electrode system. Linear sweep voltammogram performed at a scan rate of 1 mV s^{-1} on the CoPS modified GCE (Fig. S4)

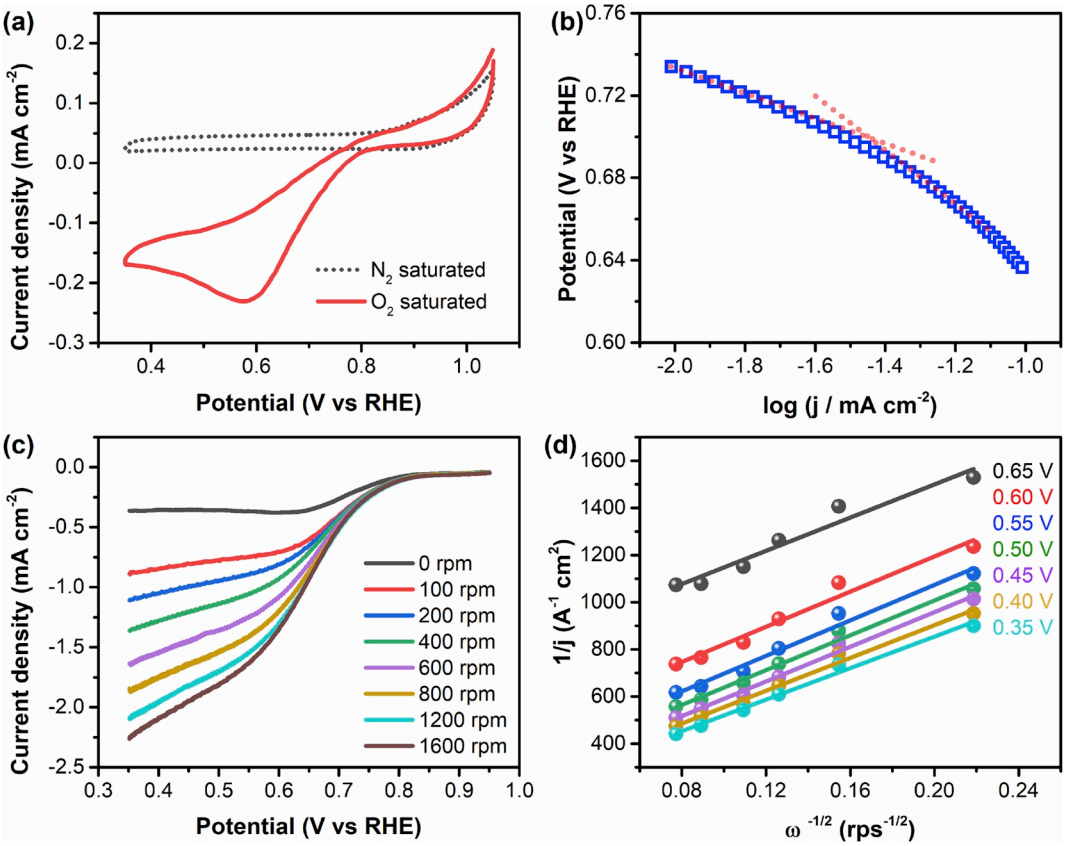

Fig. 4. Oxygen reduction reaction by CoPS coated on GC electrode to investigate the mechanism and kinetic parameters of the reaction. (a) Cyclic voltammograms of CoPS in 0.5 M KOH in presence and absence of O_2 at a scan rate of 10 mV s^{-1}. (b) Mass transport corrected Tafel plot at a scan rate of 5 mV s^{-1} and 1600 rpm rotation rate. (c) *iR* corrected linear sweep voltammograms recorded at different rotation rates using RDE starting from 0 rpm (top) to 1600 rpm (bottom) at a scan rate of 5 mV s^{-1}. (d) Corresponding K-L plots at different applied potentials.

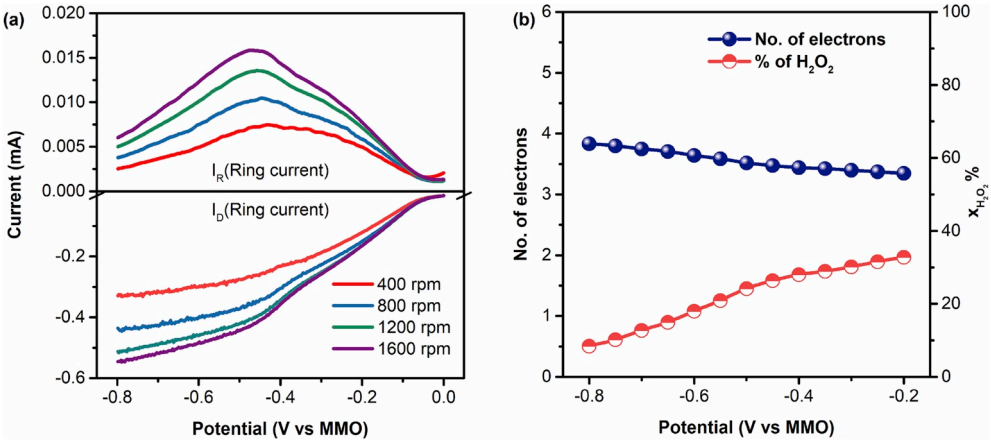

Fig. 5. (a) RRDE polarization curves for ORR of CoPS at 5 mV s^{-1} in 0.5 M KOH at different rotations from 400 to 1600 rpm. The top portion represents the ring current (due to H_2O_2 oxidation) and the bottom portion depicts the current due to oxygen reduction on the disc. The ring potential is held at 0.6 V vs MMO. (b) Number of electrons transferred and percentage of H_2O_2 produced during ORR as determined from ring and disk currents.

shows an overpotential of 415 mV to obtain 10 mA cm^{-2} current density (Tables S1 and SI). The activity is found to be improved when composites of the electrocatalyst with various carbon supports, acetylene black (AB), vulcanized carbon (VC) and reduced graphene oxide (rGO) have been used. As demonstrated in Fig. S4, the rGO composite (329 mV) is observed to have the lowest over potential to achieve 10 mA cm^{-2} followed by CoPS-VC physical mixture (400 mV). CoPS-AB physical mixture shows no change as compared to the pristine cobalt phosphosulfide.

The x-ray pattern of the catalyst after 1000 potential cycles in 0.5 M KOH shows no difference thus revealing the stability of the catalyst (Figs. S6 and SI) during OER. In addition, negligible change in potential is detected in the chronopotentiometry curve for a period of 10 h when the electrode is kept at a drain current of 10 mA cm^{-2} (Figs. S8a and SI). However, the Raman spectrum of the spent catalyst subjected to a potential of 1.6 V vs RHE for 2 h exhibits new bands in addition to the ones at 329 cm^{-1} and 436 cm^{-1} corresponding to pyrite type CoPS. The bands at 192, 476, 515, 609 and 674 cm^{-1} (Figs. S7 and SI) correspond to

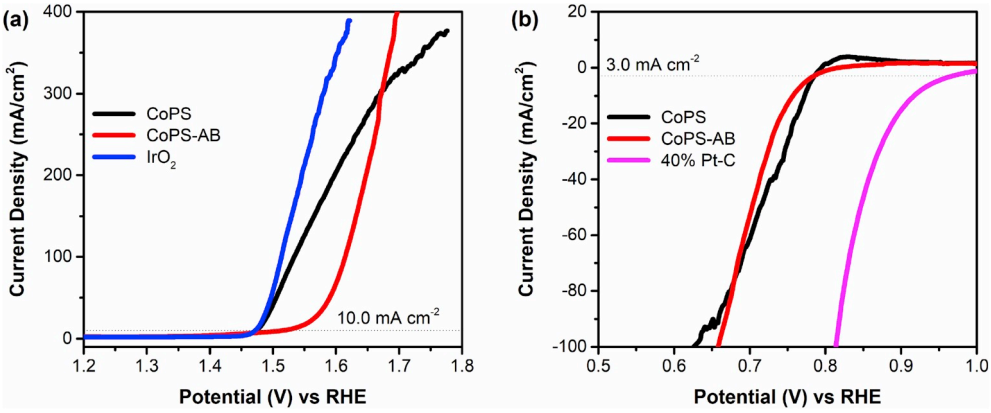

Fig. 6. iR-corrected linear sweep voltammograms recorded at 1 mV s^{-1} in 0.5 M KOH for (a) OER and (b) ORR catalyzed by CoPS and CoPS-acetylene black (AB) mixture coated on GDL electrodes as compared to IrO_2-AB for OER and 40% Pt–C for ORR.

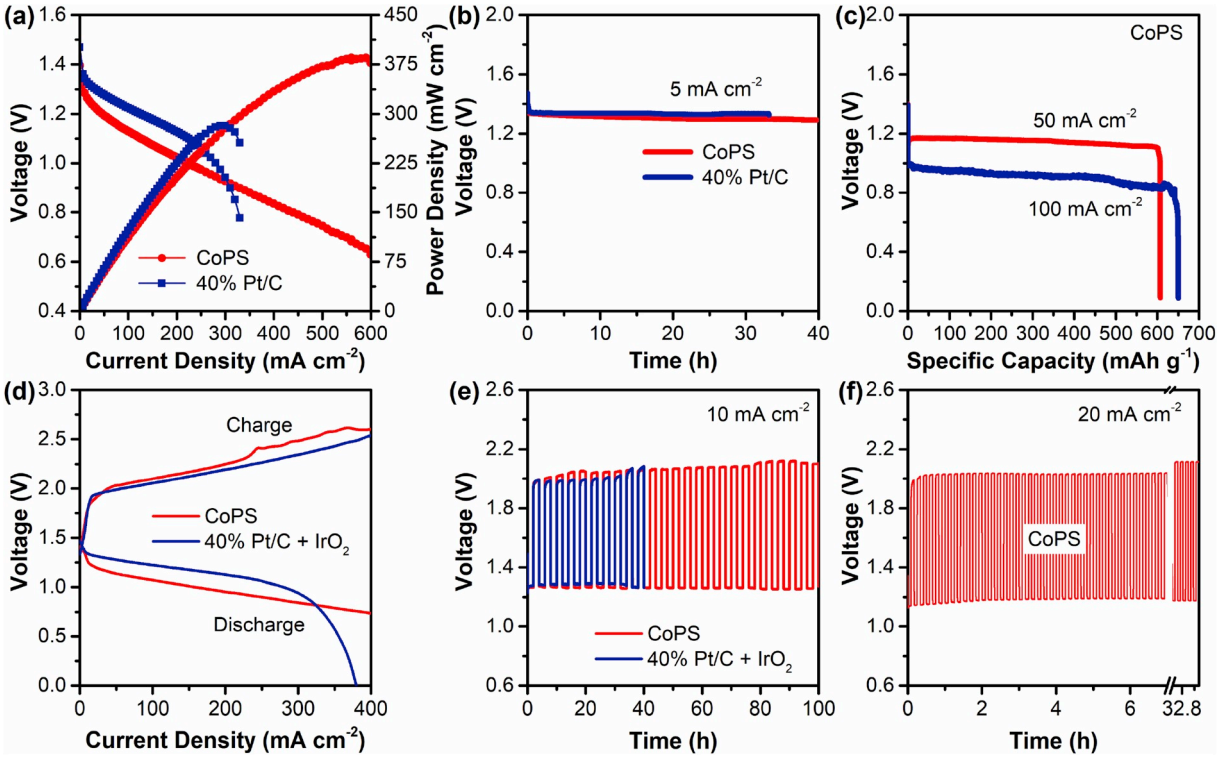

Fig. 7. (a) Polarization curves and power density plots of primary zinc-air battery using CoPS as air cathode catalyst. Commercial 40% Pt/C in KOH electrolyte is also shown for comparison. (b) Discharge curves of primary batteries using CoPS and Pt/C cathodes. (c) Specific capacities of primary batteries at two different current densities (50 mA cm^{-2} and 100 mA cm^{-2}) using CoPS as the ORR catalyst, when normalized to the mass of consumed zinc. (d) Charge and discharge polarization curves of rechargeable zinc-air battery using CoPS as compared to the one using Pt/C (ORR) and IrO_2 (OER). (e) Galvanostatic charge and discharge cycling profiles of CoPS as a bifunctional catalyst along with that of Pt/C + IrO_2 for a 4 h long cycle period at 10 mA cm^{-2} current density. (f) Short cycle period of 10 min at a high current density of 20 mA cm^{-2} is also shown.

different CoO stretching vibrations in cobalt oxy/hydroxy species [66] indicating the formation of Co_3O_4/CoOOH on the electrode surface at the onset of O_2 evolution. Co_3O_4 is known to get oxidized in alkaline electrolyte to CoOOH with anodic DC bias [67,68]. The oxy/hydroxy species act as active sites and are responsible for the enhanced electrocatalytic performance of CoPS towards OER [15,48,69–71].

3.2.3. *Bifunctional activity of the catalyst*

The reversibility of the oxygen electrode catalysis is evident from the difference (ΔE) between the potential values (at a current density of 10 mA cm^{-2}) for OER ($E_{j=10}$) and ORR half-wave potentials ($E_{1/2}$). The value (ΔE = 0.98 V) is very comparable to and even smaller than several corresponding metal oxides and certain noble metal catalyst combinations such as Pt/C and Ru/C (Tables S2 and SI). The catalyst CoPS-AB coated on GDL is used to fabricate zinc-air battery in the present studies. In addition to good OER activity, using GDL support leads to significant improvement towards ORR as well (Fig. 6). The potential required to attain a current density of 3 mA cm^{-2} ($E_{j=3}$) is found to be 0.79 V for both CoPS and CoPS-AB and the corresponding ΔE values are observed to be 0.69 V and 0.73 V respectively [between $E_{j=10}$ (OER) and $E_{j=3}$ (ORR)]. The small ΔE value (as compared to noble metal catalysts [72], oxide [72], hydroxides [73] and sulphides [22]) demonstrates the excellent bi-functional activity of CoPS towards ORR/OER in alkaline medium and makes it ideal for both aqueous and gel-based battery

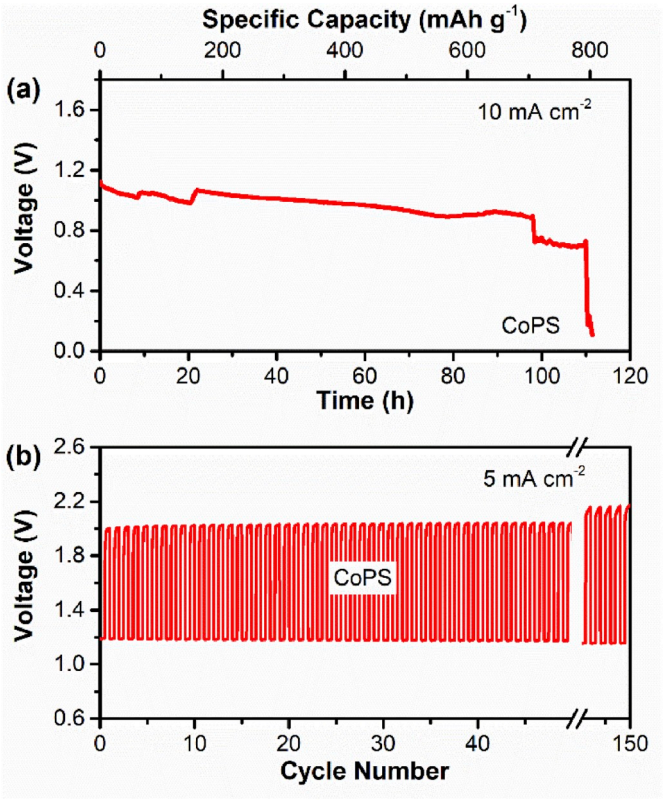

Fig. 8. (a) Galvanostatic discharge curve under a drain current of 10 mA cm^{-2} for primary zinc-air battery using CoPS as cathode catalyst in PAAK based gel electrolyte. (b) Charge-discharge profile of a rechargeable cell at 5 mA cm^{-2} current density for 10 min cycle period.

studies.

3.3. Zinc-air battery characterization

3.3.1. Primary aqueous zinc-air battery

A primary zinc-air cell is assembled using a parallel electrode assembly with CoPS coated onto gas diffusion layer (GDL) as the cathode and polished zinc plate as the anode in 6 M KOH as the electrolyte. An open circuit potential (OCP) of 1.4 V is observed. The battery delivers a peak power density of 385 mW cm^{-2} at a high current density of 560 mA cm^{-2} (Fig. 7a) and is quite comparable to the literature data (Tables S3 and SI). At 1.0 V potential, a current density of 220 mA cm^{-2} is recorded. When galvanostatically discharged at 5 mA cm^{-2} almost constant voltage plateau of 1.3 V is observed for over 40 h (Fig. 7b). The specific capacities of the cells operating at 50 mA cm^{-2} (~29 h) and 100 mA cm^{-2} (~13 h) normalized to the mass of consumed zinc are determined to be 607 mA h g^{-1} and 650 $mAhg^{-1}$, with energy densities of 675 Wh kg^{-1} and 663 Wh kg^{-1} respectively (Fig. 7c). High OCP and operational voltage values with high drain currents for long duration confirm the excellent ORR kinetics and stability of the catalyst for the primary zinc air systems.

3.3.2. Rechargeable aqueous zinc-air battery

The bifunctional aspect of CoPS is examined by fabricating a rechargeable zinc-air battery using a parallel arrangement of CoPS coated on two separate GDL electrodes (air cathodes) with a zinc plate (anode) inserted in between. Electrolyte containing 6 M KOH and 0.2 M zinc acetate is used to facilitate reversible deposition of zinc. A battery comprising commercial Pt/C for ORR and IrO_2 for OER is fabricated to obtain data for comparative purposes. Fig. 7d represents the polarization charge-discharge profiles for the batteries fabricated in the present studies. Both long term (4 h per cycle) and short term (10 min per cycle) galvanostatic charge-discharge cycling studies are performed at current densities of 10 mA cm^{-2} and 20 mA cm^{-2} respectively (Fig. 7e and f). The initial voltage polarizations are 0.71 V (4 h cycle at 10 mA cm^{-2}) and 0.84 V (10 min cycle at 20 mA cm^{-2}) corresponding to round trip efficiencies of 64.1% and 57.4% respectively (Tables S4 and SI). Experiment under high drain current of 10 mA cm^{-2} (Figs. S13a and SI) in air-breathing mode (1 h. cycle period) reveals voltage polarization of 0.77 V (with 61.1 round trip efficiency) for ~ 100 cycles with negligible change. When high drain current of 50 mA cm^{-2} is used (20 min cycling duration), the cell shows constant voltage polarization for over 100 cycles (0.84 V, Figs. S13b and SI). The Pt/C–IrO_2 based cell degrades in short time period under identical conditions (Figs. S13b and SI).

3.3.3. Gel-based zinc-air battery

With the recent growth in portable electronic devices, there has been increasing interest in flexible batteries based on gel electrolytes. The gel-electrolyte based batteries may exhibit long shelf life and cycling performance as compared to flooded cells due to low internal resistance and corrosion. The dendrite growth of zinc can also be addressed to some extent. Of course, the use of a gel electrolyte prevents problems related to leakage and improves the safety and flexibility of the battery. In the gel electrolyte presence of carboxylate groups, high segmental motion and extensive crosslinking due to the polyacrylate backbone gives rise to high ionic conductivity and mechanical strength [74–77]. The hydrophilicity of the polymer is enhanced which leads to increased water retention. The synthesized PAAK-KOH-H_2O polymer hydrogel at 7 wt % dispersion in 6 M KOH electrolyte possesses ionic conductivity of 0.169 Scm^{-1} (Figs. S9 and SI) which is comparable to that of aqueous KOH electrolyte [54]. Fig. 8a displays the galvanostatic discharge profile of a primary battery that operates for almost 112 h displaying a specific capacity of 803 mA cm^{-2} corresponding to an energy density of 891 Wh kg^{-1}. This is an immense improvement as compared to the aqueous electrolyte-based batteries. The charge-discharge cycles for the rechargeable battery at a current density of 5 $mAcm^{-2}$ for 10 min cycle period (Fig. 8b) shows voltage polarization of 0.80 V with round trip efficiency 60.0%. This is quite comparable to that of aqueous liquid-based batteries. The comparison of the SEM images of the used zinc electrodes reveals that dendrite formation and possibly corrosion are reduced in presence of gel at the electrode as compared to liquid electrolyte (Figs. S14 and SI).

4. Summary

Highly crystalline CoPS synthesized by a solid-state technique shows bifunctionality towards oxygen electrocatalysis in alkaline electrolyte. CoPS on GDL exhibits an overpotential of 243 mV at 10 $mAcm^{-2}$ for OER which is one of the lowest reported in literature among phosphides, sulphides and phosphosulphides. The facile kinetics is found to be promoted by the formation of cobalt oxy/hydroxy species during cycling. Incorporation of P leads enhanced the covalency in the metal ligand bond and thus the stability of the catalyst. The synergistic effect of P and S in the phosphosulphide is responsible for good ORR kinetics as the phosphorus atoms get polarized by surrounding sulphur atoms increasing the adsorption of O_2 leading to a 4 electron pathway. The ORR and OER activity of CoPS is quite comparable to that of the noble metal catalysts (Pt/C–IrO_2). The bifunctional activity is exploited in zinc-air primary and rechargeable batteries in aqueous liquid and gel based alkaline electrolytes. The primary gel battery displays a specific capacity of 803 $mAcm^{-2}$ corresponding to an energy density of 891 Wh kg^{-1}. Round trip efficiency of 61% with stability over 100 h in air breathing mode has been observed for the rechargeable battery at 10 $mAcm^{-2}$. CoPS outperforms the commercial catalysts in battery characteristics. The CoPS catalyst is economically viable for applications in flexible energy storage and energy conversion devices.

Declaration of competing interest

There are no conflicts to declare.

Acknowledgements

The authors thank DST, New Delhi and CERDEC for research funds.

Appendix A. Supplementary data

Supplementary data to this article can be found online at https://doi.org/10.1016/j.jpowsour.2019.227661.

References

[1] M. Armand, J.-M. Tarascon, Building better batteries, Nature 451 (2008) 652–657, https://doi.org/10.1038/451652a.
[2] R. Van Noorden, The rechargeable revolution: a better battery, Nature 507 (2014) 26–28, https://doi.org/10.1038/507026a.
[3] Y. Li, J. Lu, Metal–air batteries: will they Be the future electrochemical energy storage device of choice? ACS Energy Lett 2 (2017) 1370–1377, https://doi.org/10.1021/acsenergylett.7b00119.
[4] K.M. Abraham, Prospects and limits of energy storage in batteries, J. Phys. Chem. Lett. 6 (2015) 830–844, https://doi.org/10.1021/jz5026273.
[5] L. Grande, E. Paillard, J. Hassoun, J.-B. Park, Y.-J. Lee, Y.-K. Sun, S. Passerini, B. Scrosati, The lithium/air battery: Still an emerging system or a practical reality? Adv. Mater. 27 (2015) 784–800, https://doi.org/10.1002/adma.201403064.
[6] T. Ogasawara, A. Débart, M. Holzapfel, P. Novák, P.G. Bruce, Rechargeable Li 2 O 2 electrode for lithium batteries, J. Am. Chem. Soc. 128 (2006) 1390–1393, https://doi.org/10.1021/ja056811q.
[7] V.G. Anju, R. Manjunatha, P.M. Austeria, S. Sampath, Primary and rechargeable zinc–air batteries using ceramic and highly stable TiCN as an oxygen reduction reaction electrocatalyst, J. Mater. Chem. A. 4 (2016) 5258–5264, https://doi.org/10.1039/C6TA00377J.
[8] R.P. Hamlen, E.C. Jerabek, J.C. Ruzzo, E.G. Siwek, Anodes for refuelable magnesium-air batteries, J. Electrochem. Soc. 116 (1969) 1588–1592, https://doi.org/10.1149/1.2411622.
[9] S. Kukunuri, K. Naik, S. Sampath, Effects of composition and nanostructuring of palladium selenide phases, Pd 4 Se, Pd 7 Se 4 and Pd 17 Se 15 , on ORR activity and their use in Mg–air batteries, J. Mater. Chem. A. 5 (2017) 4660–4670, https://doi.org/10.1039/C7TA00253J.
[10] Y. Li, H. Dai, Recent advances in zinc–air batteries, Chem. Soc. Rev. 43 (2014) 5257–5275, https://doi.org/10.1039/C4CS00015C.
[11] G. Toussaint, P. Stevens, L. Akrour, R. Rouget, F. Fourgeot, Development of a rechargeable zinc-air battery, ECS Trans 28 (2010) 25–34, https://doi.org/10.1149/1.3507924.
[12] J. Zhang, M.B. Vukmirovic, Y. Xu, M. Mavrikakis, R.R. Adzic, Controlling the catalytic activity of platinum-monolayer electrocatalysts for oxygen reduction with different substrates, Angew. Chem. Int. Ed. 44 (2005) 2132–2135, https://doi.org/10.1002/anie.200462335.
[13] K. Yamamoto, T. Imaoka, W.-J. Chun, O. Enoki, H. Katoh, M. Takenaga, A. Sonoi, Size-specific catalytic activity of platinum clusters enhances oxygen reduction reactions, Nat. Chem. 1 (2009) 397–402, https://doi.org/10.1038/nchem.288.
[14] Y. Lee, J. Suntivich, K.J. May, E.E. Perry, Y. Shao-Horn, Synthesis and activities of rutile IrO 2 and RuO 2 nanoparticles for oxygen evolution in acid and alkaline solutions, J. Phys. Chem. Lett. 3 (2012) 399–404, https://doi.org/10.1021/jz2016507.
[15] I.C. Man, H.-Y. Su, F. Calle Vallejo, H.A. Hansen, J.I. Martínez, N.G. Inoglu, J. Kitchin, T.F. Jaramillo, J.K. Nørskov, J. Rossmeisl, Universality in oxygen evolution electrocatalysis on oxide surfaces, ChemCatChem 3 (2011) 1159–1165, https://doi.org/10.1002/cctc.201000397.
[16] J.-F. Drillet, F. Holzer, T. Kallis, S. Müller, V.M. Schmidt, Influence of CO2 on the stability of bifunctional oxygen electrodes for rechargeable zinc/air batteries and study of different CO2 filter materials, Phys. Chem. Chem. Phys. 3 (2001) 368–371, https://doi.org/10.1039/b005523i.
[17] A. Weidenkaff, S.G. Ebbinghaus, T. Lippert, Ln 1 - x A x CoO 3 (Ln = Er, La; A = Ca, Sr)/Carbon nanotube composite materials applied for rechargeable Zn/air batteries, Chem. Mater. 14 (2002) 1797–1805, https://doi.org/10.1021/cm011305v.
[18] J.-I. Jung, M. Risch, S. Park, M.G. Kim, G. Nam, H.-Y. Jeong, Y. Shao-Horn, J. Cho, Optimizing nanoparticle perovskite for bifunctional oxygen electrocatalysis, Energy Environ. Sci. 9 (2016) 176–183, https://doi.org/10.1039/C5EE03124A.
[19] X. Zhang, R. Liu, Y. Zang, G. Liu, G. Wang, Y. Zhang, H. Zhang, H. Zhao, Co/CoO nanoparticles immobilized on Co–N-doped carbon as trifunctional electrocatalysts for oxygen reduction, oxygen evolution and hydrogen evolution reactions, Chem. Commun. 52 (2016) 5946–5949, https://doi.org/10.1039/C6CC02513G.
[20] L.N. Han, L.B. Lv, Q.C. Zhu, X. Wei, X.H. Li, J.S. Chen, Ultra-durable two-electrode Zn-air secondary batteries based on bifunctional titania nanocatalysts: a Co2+ dopant boosts the electrochemical activity, J. Mater. Chem. A. 4 (2016) 7841–7847, https://doi.org/10.1039/c6ta02143c.
[21] X. Chia, A.Y.S. Eng, A. Ambrosi, S.M. Tan, M. Pumera, Electrochemistry of nanostructured layered transition-metal dichalcogenides, Chem. Rev. 115 (2015) 11941–11966, https://doi.org/10.1021/acs.chemrev.5b00287.
[22] P. Ganesan, M. Prabu, J. Sanetuntikul, S. Shanmugam, Cobalt sulfide nanoparticles grown on nitrogen and Sulfur codoped graphene oxide: an efficient electrocatalyst for oxygen reduction and evolution reactions, ACS Catal. 5 (2015) 3625–3637, https://doi.org/10.1021/acscatal.5b00154.
[23] X. Zheng, X. Han, H. Liu, J. Chen, D. Fu, J. Wang, C. Zhong, Y. Deng, W. Hu, Controllable synthesis of Ni x Se ($0.5 \leq x \leq 1$) nanocrystals for efficient rechargeable zinc–air batteries and water splitting, ACS Appl. Mater. Interfaces 10 (2018) 13675–13684, https://doi.org/10.1021/acsami.8b01651.
[24] L.A. Stern, L. Feng, F. Song, X. Hu, Ni 2 P as a Janus catalyst for water splitting: the oxygen evolution activity of Ni 2 P nanoparticles, Energy Environ. Sci. 8 (2015) 2347–2351, https://doi.org/10.1039/C5EE01155H.
[25] K. Chen, X. Huang, C. Wan, H. Liu, Hybrids based on transition metal phosphide (Mn 2 P, Co 2 P, Ni 2 P) nanoparticles and heteroatom-doped carbon nanotubes for efficient oxygen reduction reaction, RSC Adv. 5 (2015) 92893–92898, https://doi.org/10.1039/C5RA21385A.
[26] H. Li, Q. Li, P. Wen, T.B. Williams, S. Adhikari, C. Dun, C. Lu, D. Itanze, L. Jiang, D. L. Carroll, G.L. Donati, P.M. Lundin, Y. Qiu, S.M. Geyer, Colloidal cobalt phosphide nanocrystals as trifunctional electrocatalysts for overall water splitting powered by a zinc-air battery, Adv. Mater. 30 (2018) 1705796, https://doi.org/10.1002/adma.201705796.
[27] S. Anantharaj, S.R. Ede, K. Sakthikumar, K. Karthick, S. Mishra, S. Kundu, Recent trends and perspectives in electrochemical water splitting with an emphasis on sulfide, selenide, and phosphide catalysts of Fe, Co, and Ni: a review, ACS Catal. 6 (2016) 8069–8097, https://doi.org/10.1021/acscatal.6b02479.
[28] J.D. Wiensch, J. John, J.M. Velazquez, D.A. Torelli, A.P. Pieterick, M.T. McDowell, K. Sun, X. Zhao, B.S. Brunschwig, N.S. Lewis, Comparative study in acidic and alkaline media of the effects of pH and crystallinity on the hydrogen-evolution reaction on MoS 2 and MoSe 2, ACS Energy Lett 2 (2017) 2234–2238, https://doi.org/10.1021/acsenergylett.7b00700.
[29] M.-R. Gao, J. Jiang, S.-H. Yu, Solution-based synthesis and design of late transition metal chalcogenide materials for oxygen reduction reaction (ORR), Small 8 (2012) 13–27, https://doi.org/10.1002/smll.201101573.
[30] Y. Zhang, L. Gao, E.J.M. Hensen, J.P. Hofmann, Evaluating the stability of Co 2 P electrocatalysts in the hydrogen evolution reaction for both acidic and alkaline electrolytes, ACS Energy Lett 3 (2018) 1360–1365, https://doi.org/10.1021/acsenergylett.8b00514.
[31] J.F. Callejas, J.M. McEnaney, C.G. Read, J.C. Crompton, A.J. Biacchi, E.J. Popczun, T.R. Gordon, N.S. Lewis, R.E. Schaak, Electrocatalytic and photocatalytic hydrogen production from acidic and neutral-pH aqueous solutions using iron phosphide nanoparticles, ACS Nano 8 (2014) 11101–11107, https://doi.org/10.1021/nn5048553.
[32] J. Xu, J. Li, D. Xiong, B. Zhang, Y. Liu, K.-H. Wu, I. Amorim, W. Li, L. Liu, Trends in activity for the oxygen evolution reaction on transition metal (M = Fe, Co, Ni) phosphide pre-catalysts, Chem. Sci. 9 (2018) 3470–3476, https://doi.org/10.1039/C7SC05033J.
[33] H. Liang, A.N. Gandi, D.H. Anjum, X. Wang, U. Schwingenschlögl, H.N. Alshareef, Plasma-assisted synthesis of NiCoP for efficient overall water splitting, Nano Lett. 16 (2016) 7718–7725, https://doi.org/10.1021/acs.nanolett.6b03803.
[34] X. Wu, X. Han, X. Ma, W. Zhang, Y. Deng, C. Zhong, W. Hu, Morphology-controllable synthesis of Zn–Co-mixed sulfide nanostructures on carbon fiber paper toward efficient rechargeable zinc–air batteries and water electrolysis, ACS Appl. Mater. Interfaces 9 (2017) 12574–12583, https://doi.org/10.1021/acsami.6b16602.
[35] M. Shen, C. Ruan, Y. Chen, C. Jiang, K. Ai, L. Lu, Covalent entrapment of cobalt–iron sulfides in N-doped mesoporous carbon: extraordinary bifunctional electrocatalysts for oxygen reduction and evolution reactions, ACS Appl. Mater. Interfaces 7 (2015) 1207–1218, https://doi.org/10.1021/am507033x.
[36] C.C. Mayorga-Martinez, Z. Sofer, D. Sedmidubský, Š. Huber, A.Y.S. Eng, M. Pumera, Layered metal thiophosphite materials: magnetic, electrochemical, and electronic properties, ACS Appl. Mater. Interfaces 9 (2017) 12563–12573, https://doi.org/10.1021/acsami.6b16553.
[37] D. Mukherjee, M.A. P, S. Sampath, Few-layer iron Selenophosphate, FePSe 3 : efficient electrocatalyst toward water splitting and oxygen reduction reactions, ACS Appl. Energy Mater. 1 (2018) 220–231, https://doi.org/10.1021/acsaem.7b00101.
[38] J. Luo, H. Wang, G. Su, Y. Tang, H. Liu, F. Tian, D. Li, Self-supported nickel phosphosulphide nanosheets for highly efficient and stable overall water splitting, J. Mater. Chem. A. 5 (2017) 14865–14872, https://doi.org/10.1039/C7TA02651J.
[39] Y. Tang, F. Jing, Z. Xu, F. Zhang, Y. Mai, D. Wu, Highly crumpled hybrids of nitrogen/sulfur dual-doped graphene and Co 9 S 8 nanoplates as efficient bifunctional oxygen electrocatalysts, ACS Appl. Mater. Interfaces 9 (2017) 12340–12347, https://doi.org/10.1021/acsami.6b15461.
[40] X. Han, X. Wu, C. Zhong, Y. Deng, N. Zhao, W. Hu, NiCo 2 S 4 nanocrystals anchored on nitrogen-doped carbon nanotubes as a highly efficient bifunctional electrocatalyst for rechargeable zinc-air batteries, Nano Energy 31 (2017) 541–550, https://doi.org/10.1016/j.nanoen.2016.12.008.
[41] B. Chen, R. Li, G. Ma, X. Gou, Y. Zhu, Y. Xia, Cobalt sulfide/N,S codoped porous carbon core–shell nanocomposites as superior bifunctional electrocatalysts for oxygen reduction and evolution reactions, Nanoscale 7 (2015) 20674–20684, https://doi.org/10.1039/C5NR07429K.
[42] J. Kibsgaard, T.F. Jaramillo, Molybdenum phosphosulfide: an active, acid-stable, earth-abundant catalyst for the hydrogen evolution reaction, Angew. Chem. Int. Ed. 53 (2014) 14433–14437, https://doi.org/10.1002/anie.201408222.

[43] W. Liu, E. Hu, H. Jiang, Y. Xiang, Z. Weng, M. Li, Q. Fan, X. Yu, E.I. Altman, H. Wang, A highly active and stable hydrogen evolution catalyst based on pyrite-structured cobalt phosphosulfide, Nat. Commun. 7 (2016) 10771, https://doi.org/10.1038/ncomms10771.
[44] R. Ye, P. del Angel-Vicente, Y. Liu, M.J. Arellano-Jimenez, Z. Peng, T. Wang, Y. Li, B.I. Yakobson, S.-H. Wei, M.J. Yacaman, J.M. Tour, High-performance hydrogen evolution from MoS 2(1- x) P x solid solution, Adv. Mater. 28 (2016) 1427–1432, https://doi.org/10.1002/adma.201504866.
[45] H. Huang, X. Feng, C. Du, W. Song, High-quality phosphorus-doped MoS 2 ultrathin nanosheets with amenable ORR catalytic activity, Chem. Commun. 51 (2015) 7903–7906, https://doi.org/10.1039/C5CC01841B.
[46] Q. Shen, J. Yang, K.L. Chen, H. Wang, J.B. Liu, H. Yan, Co3O4nanorods–graphene composites as catalysts for rechargeable zinc-air battery, J. Solid State Electrochem. 20 (2016) 3331–3336, https://doi.org/10.1007/s10008-016-3299-z.
[47] N. Wang, L. Li, D. Zhao, X. Kang, Z. Tang, S. Chen, Graphene composites with cobalt sulfide: efficient trifunctional electrocatalysts for oxygen reversible catalysis and hydrogen production in the same electrolyte, Small 13 (2017) 1701025, https://doi.org/10.1002/smll.201701025.
[48] M.W. Kanan, D.G. Nocera, In situ formation of an oxygen-evolving catalyst in neutral water containing phosphate and Co2+, Science (80-.) 321 (2008) 1072–1075, https://doi.org/10.1126/science.1162018.
[49] C.-Z. Yuan, Y.-F. Jiang, Z. Wang, X. Xie, Z.-K. Yang, A. Bin Yousaf, A.-W. Xu, Cobalt phosphate nanoparticles decorated with nitrogen-doped carbon layers as highly active and stable electrocatalysts for the oxygen evolution reaction, J. Mater. Chem. A. 4 (2016) 8155–8160, https://doi.org/10.1039/C6TA01929C.
[50] M. Cabán-Acevedo, M.L. Stone, J.R. Schmidt, J.G. Thomas, Q. Ding, H.-C. Chang, M.-L. Tsai, J.-H. He, S. Jin, Efficient hydrogen evolution catalysis using ternary pyrite-type cobalt phosphosulphide, Nat. Mater. 14 (2015) 1245–1251, https://doi.org/10.1038/nmat4410.
[51] Z. Liu, J. Zhang, Y. Liu, W. Zhu, X. Zhang, Q. Wang, Electrodeposition of cobalt phosphosulfide nanosheets on carbon fiber paper as efficient electrocatalyst for oxygen evolution, ChemElectroChem 5 (2018) 1677–1682, https://doi.org/10.1002/celc.201800384.
[52] J. Li, Z. Xia, X. Zhou, Y. Qin, Y. Ma, Y. Qu, Quaternary pyrite-structured nickel/cobalt phosphosulfide nanowires on carbon cloth as efficient and robust electrodes for water electrolysis, Nano Res 10 (2017) 814–825, https://doi.org/10.1007/s12274-016-1335-z.
[53] Z. Dai, H. Geng, J. Wang, Y. Luo, B. Li, Y. Zong, J. Yang, Y. Guo, Y. Zheng, X. Wang, Q. Yan, Hexagonal-phase cobalt monophosphosulfide for highly efficient overall water splitting, ACS Nano 11 (2017) 11031–11040, https://doi.org/10.1021/acsnano.7b05050.
[54] C. Iwakura, H. Wada, S. Nohara, N. Furukawa, H. Inoue, M. Morita, New electric double layer capacitor with polymer hydrogel electrolyte, Electrochim. Acta 48 (2003) 749–753, https://doi.org/10.1149/1.1535752.
[55] J.F. Moulder, W.F. Stickle, P.E. Sobol, K.D. Bomben, Handbook of X-Ray Photoelectron Spectroscopy, Perkin-Elmer Corporation, 1992.
[56] M.C. Biesinger, B.P. Payne, A.P. Grosvenor, L.W.M. Lau, A.R. Gerson, R.S.C. Smart, Resolving surface chemical states in XPS analysis of first row transition metals, oxides and hydroxides: Cr, Mn, Fe, Co and Ni, Appl. Surf. Sci. 257 (2011) 2717–2730, https://doi.org/10.1016/j.apsusc.2010.10.051.
[57] J.F. Callejas, C.G. Read, E.J. Popczun, J.M. McEnaney, R.E. Schaak, Nanostructured Co 2 P electrocatalyst for the hydrogen evolution reaction and direct comparison with morphologically equivalent CoP, Chem. Mater. 27 (2015) 3769–3774, https://doi.org/10.1021/acs.chemmater.5b01284.
[58] C. Song, J. Zhang, Electrocatalytic oxygen reduction reaction, in: J. Zhang (Ed.), PEM Fuel Cell Electrocatal. Catal. Layers, Springer London, London, 2008, pp. 89–134, https://doi.org/10.1007/978-1-84800-936-3_2.
[59] X. Ge, A. Sumboja, D. Wuu, T. An, B. Li, F.W.T. Goh, T.S.A. Hor, Y. Zong, Z. Liu, Oxygen reduction in alkaline media: from mechanisms to recent advances of catalysts, ACS Catal. 5 (2015) 4643–4667, https://doi.org/10.1021/acscatal.5b00524.
[60] E. Davari, D.G. Ivey, Bifunctional electrocatalysts for Zn–air batteries, Sustain. Energy Fuels. 2 (2018) 39–67, https://doi.org/10.1039/C7SE00413C.
[61] N.M. Marković, T.J. Schmidt, V. Stamenković, P.N. Ross, Oxygen reduction reaction on Pt and Pt bimetallic surfaces: a selective review, Fuel Cells 1 (2001) 105–116, https://doi.org/10.1002/1615-6854(200107)1:2<105::AID-FUCE105>3.0.CO;2-9.
[62] X. Li, W. Qu, J. Zhang, H. Wang, Electrocatalytic activities of La0.6Ca0.4CoO3 and La0.6Ca0.4CoO3-carbon composites toward the oxygen reduction reaction in concentrated alkaline electrolytes, J. Electrochem. Soc. 158 (2011) A597–A604, https://doi.org/10.1149/1.3560170.
[63] E. Farjami, L.J. Deiner, Kinetic study of the oxygen reduction reaction on α-Ni(OH) 2 and α-Ni(OH) 2 supported on graphene oxide, J. Electrochem. Soc. 162 (2015) H571–H578, https://doi.org/10.1149/2.0041509jes.
[64] A.P. Periasamy, W.-P. Wu, G.-L. Lin, Z.-Y. Shih, Z. Yang, H.-T. Chang, Synthesis of Cu 9 S 8/carbon nanotube nanocomposites with high electrocatalytic activity for the oxygen reduction reaction, J. Mater. Chem. A. 2 (2014) 11899, https://doi.org/10.1039/C4TA01713G.
[65] A.Y.S. Eng, A. Ambrosi, Z. Sofer, P. Šimek, M. Pumera, Electrochemistry of transition metal dichalcogenides: strong dependence on the metal-to-chalcogen composition and exfoliation method, ACS Nano 8 (2014) 12185–12198, https://doi.org/10.1021/nn503832j.
[66] J. Yang, H. Liu, W.N. Martens, R.L. Frost, Synthesis and characterization of cobalt hydroxide, cobalt oxyhydroxide, and cobalt oxide nanodiscs, J. Phys. Chem. C 114 (2010) 111–119, https://doi.org/10.1021/jp908548f.
[67] M. Hamdani, R.N. Singh, P. Chartier, Co3O4 and Co- based spinel oxides bifunctional oxygen electrodes, Int. J. Electrochem. Sci. 5 (2010) 556–577.
[68] N. Jiang, B. You, M. Sheng, Y. Sun, Electrodeposited cobalt-phosphorous-derived films as competent bifunctional catalysts for overall water splitting, Angew. Chem. Int. Ed. 54 (2015) 6251–6254, https://doi.org/10.1002/anie.201501616.
[69] M. Bajdich, M. García-Mota, A. Vojvodic, J.K. Nørskov, A.T. Bell, Theoretical investigation of the activity of cobalt oxides for the electrochemical oxidation of water, J. Am. Chem. Soc. 135 (2013) 13521–13530, https://doi.org/10.1021/ja405997s.
[70] B.S. Yeo, A.T. Bell, Enhanced activity of gold-supported cobalt oxide for the electrochemical evolution of oxygen, J. Am. Chem. Soc. 133 (2011) 5587–5593, https://doi.org/10.1021/ja200559j.
[71] M. Zhang, M. de Respinis, H. Frei, Time-resolved observations of water oxidation intermediates on a cobalt oxide nanoparticle catalyst, Nat. Chem. 6 (2014) 362–367, https://doi.org/10.1038/nchem.1874.
[72] T. Li, Y. Lu, S. Zhao, Z. Da Gao, Y.Y. Song, Co3O4-doped Co/CoFe nanoparticles encapsulated in carbon shells as bifunctional electrocatalysts for rechargeable Zn-Air batteries, J. Mater. Chem. A. 6 (2018) 3730–3737, https://doi.org/10.1039/c7ta11171a.
[73] Y. Zhan, G. Du, S. Yang, C. Xu, M. Lu, Z. Liu, J.Y. Lee, Development of cobalt hydroxide as a bifunctional catalyst for oxygen electrocatalysis in alkaline solution, ACS Appl. Mater. Interfaces 7 (2015) 12930–12936, https://doi.org/10.1021/acsami.5b02670.
[74] C. Iwakura, The possible use of polymer gel electrolytes in nickel/metal hydride battery, Solid State Ion. 148 (2002) 487–492, https://doi.org/10.1016/S0167-2738(02)00092-9.
[75] H. Gao, K. Lian, Proton-conducting polymer electrolytes and their applications in solid supercapacitors: a review, RSC Adv. 4 (2014) 33091–33113, https://doi.org/10.1039/C4RA05151C.
[76] X. Zhu, H. Yang, Y. Cao, X. Ai, Preparation and electrochemical characterization of the alkaline polymer gel electrolyte polymerized from acrylic acid and KOH solution, Electrochim. Acta 49 (2004) 2533–2539, https://doi.org/10.1016/j.electacta.2004.02.008.
[77] R. Palaniappan, G.G. Botte, Efficacy of potassium poly(acrylate) gel electrolyte as a substitute to aqueous electrolytes for alkaline ammonia electrolysis, Electrochim. Acta 88 (2013) 772–781, https://doi.org/10.1016/j.electacta.2012.10.023.